
Subhomogeneous Deep Equilibrium Models

Pietro Sittoni^{*1} Francesco Tudisco^{*1,2}

Abstract

Implicit-depth neural networks have grown as powerful alternatives to traditional networks in various applications in recent years. However, these models often lack guarantees of existence and uniqueness, raising stability, performance, and reproducibility issues. In this paper, we present a new analysis of the existence and uniqueness of fixed points for implicit-depth neural networks based on the concept of subhomogeneous operators and the nonlinear Perron-Frobenius theory. Compared to previous similar analyses, our theory allows for weaker assumptions on the parameter matrices, thus yielding a more flexible framework for well-defined implicit networks. We illustrate the performance of the resulting subhomogeneous networks on feed-forward, convolutional, and graph neural network examples.

1. Introduction

Implicit-depth Neural Networks (NNs) have emerged as powerful tools in deep learning. Rather than using a sequence of nested layers, these models define feature embeddings as the solution to specific nonlinear equations. Two popular examples of implicit-depth networks are Neural ODEs (Chen et al., 2018), whose output is calculated by solving an ordinary differential equation, and Deep Equilibrium (DEQ) Models (Bai et al., 2019), which define the output in terms of a fixed-point equation. These approaches have a number of advantages as (a) they have been shown to match or even exceed the performance of traditional NNs on several tasks, including time series and sequence modeling (Bai et al., 2019; Rusch & Mishra, 2021), and (b) memory-wise, they are more efficient than traditional NNs as backpropagation is done analytically and does not require to store internal weights, allowing to handle deep NN architectures more efficiently.

^{*}Equal contribution ¹Gran Sasso Science Institute, L'Aquila, Italy ²School of Mathematics and Maxwell Institute, University of Edinburgh, Edinburgh, UK. Correspondence to: Pietro Sittoni <pietro.sittoni@gssi.it>, Francesco Tudisco <f.tudisco@ed.ac.uk>.

DEQ models can be viewed as infinite-depth feed-forward neural networks, with weight tying, i.e. where the same transformation is used on each layer (Dabre & Fujita, 2019; Dehghani et al., 2019). Indeed, in this type of model, the evaluation of the network is executed by solving a fixed-point equation $z = f_\theta(z; x)$ which can be thought of as the limit for the number of layers $n \rightarrow \infty$ of an n -deep network $z^{(n)} = f_\theta(z^{(n-1)}; x)$. As the network is now implicitly defined as the solution of the equation $f_\theta(z; x) - z = 0$, one can use the Implicit Function Theorem to compute and propagate the gradients, thus reducing the memory cost with respect to standard backpropagation (Bai et al., 2019; 2020).

Despite their potential advantages, not all DEQ models are well-defined. In fact, one of the main open questions for DEQ architectures is whether any fixed point actually exists and whether this is unique. Lack of uniqueness, in particular, can be a problem as for a given data x and fixed pre-trained weights θ , the resulting fixed-point embedding z may change, raising stability, performance, and reproducibility issues. These potential drawbacks are often ignored or addressed only via empirical arguments based on experimental evidence that deep networks work well in practice. The most prominent line of analysis of uniqueness for deep equilibrium fixed points is based on monotone operator theory (Winston & Kolter, 2020; Ryu & Boyd, 2016). While elegant and efficient, monotone operator DEQs (MonDEQs) require special parametrizations of the layer weights to guarantee the DEQ model f_θ is operator monotone.

In this work, we present a new analysis of existence and uniqueness of DEQ fixed points based on positive, subhomogeneous operators. Using the Thomson projective metric and techniques from nonlinear Perron-Frobenius theory (Lemmens & Nussbaum, 2012; Gautier et al., 2019), we provide a new theorem showing that a broad class of operators f_θ admits unique fixed points. In particular, we show that our uniqueness theorem holds for several example architectures of the form $f_\theta(z; x) = \sigma(Wz + \text{MLP}(x))$, with commonly used activation functions σ , provided a suitable homogeneous layer normalization is added as final layer. This result allows us to design stable DEQ models with a well-posed fixed-point equation which we illustrate how to practically implement.

Our theoretical findings are complemented by several ex-

perimental evaluations where we compare simple fully-connected and convolutional DEQ architectures based on monotone operators with the newly introduced subhomogeneous deep equilibrium model (SubDEQ) on benchmark image classification tasks.

2. Related work

The classical approach to layer design in deep learning is based on explicitly defined function compositions and the corresponding computational graph. In contrast, implicit-depth approaches do not explicitly define the computational graph and define the model implicitly as the solution of a specific equation. The computational graph needs then to be extracted from the implicit formulation. NeuralODE is a popular example where the model is defined as the solution of an ordinary differential equation and backpropagation can be implemented via the adjoint method (Chen et al., 2018). Another example is the DEQ, where the model is defined as the fixed point of a nonlinear function and backpropagation can be done using the implicit function theorem (Bai et al., 2019). However, DEQ may not be well-posed, as fixed points of nonlinear mappings may not exist or may not be unique. Several works in the literature propose variations of DEQ architecture with criteria for certified well-posedness using different methods, including monDEQ (Winston & Kolter, 2020) based on monotone operator theory, applying contraction theory (Jafarpour et al., 2022), using an over-parametrized DEQ with a condition on the initial equilibrium point, or exploiting linear Perron-Frobenius theory on graph neural networks, (Gu et al., 2021; Ghaoui et al., 2020). Just like standard explicit networks, DEQ models are vulnerable to adversarial input perturbations (Yang et al., 2022) and well-posed parameterizations may improve the robustness of the model. For example, using semialgebraic representation of monDEQ, (Chen et al., 2021) showed that monDEQ are more robust to l^2 perturbation. Similarly, (Wei & Kolter, 2022) showed that unlike generic DEQs, monDEQ can achieve comparable l^∞ certified robustness to similarly-sized fully explicit networks, via interval bound propagation. Finally, we highlight that models based on DEQ architectures have been successfully employed in a wide range of specific applications. The first competitive performance was shown in the sequence modeling domain (Bai et al., 2019; 2020). Soon after that, efficient DEQ models have been designed for inverse problems in imaging (Gilton et al., 2021)(Zhao et al., 2023), image denoising (Chen et al., 2023), optical flow estimation (Bai et al., 2022), landmark detection (Micaelli et al., 2023), semantic segmentation (Bai et al., 2020), and generative modeling using a diffusion-based approach (Pogle et al., 2022).

3. Subhomogeneous operators

The fundamental brick of our analysis is the notion of subhomogeneous operator. Recall that an operator $F : \mathbb{R}^n \rightarrow \mathbb{R}^n$ is (positively) μ -homogeneous, for some $\mu > 0$ if $F(\alpha z) = \alpha^\mu F(z)$ for all positive coefficients $\alpha > 0$ and all entrywise positive vectors $z > 0$. When F is differentiable, Euler’s theorem for homogeneous functions provides an elegant equivalent characterization of homogeneous operators as the set of F such that the identity $F'(z)z = \mu F(z)$ holds for all z , where $F'(z)$ denotes the Jacobian of F in z . The proposed notion of subhomogeneous operators generalizes the concept of homogeneous mappings, starting from this second characterization.

Definition 3.1 (Subhomogeneous operator). Let $F : \mathbb{R}^n \rightarrow \mathbb{R}^n$ be a Lipschitz mapping. For a coefficient $\mu > 0$ and $\Omega \subseteq \text{dom}_+(F) := \{z \in \mathbb{R}^n \mid F(z) > 0\}$, we say that F is μ -subhomogeneous in Ω , briefly $F \in \text{subhom}_\mu(\Omega)$, if

$$|Mz| \leq \mu F(z), \quad (1)$$

for all $z \in \Omega$ and all $M \in \partial F(z)$, where $\partial F(z)$ denotes Clarke’s generalized Jacobian of F at the point z , and where all the inequalities, as well as the absolute value, are meant entrywise. Similarly, we say that F is strongly μ -subhomogeneous in Ω , briefly $F \in \text{s-subhom}_\mu(\Omega)$, if

$$|M| |z| \leq \mu F(z), \quad (2)$$

for all $z \in \Omega$ and all $M \in \partial F(z)$.

Subhomogeneity generalizes both homogeneity and strong-subhomogeneity. In fact, all μ -homogeneous differentiable operators are μ -subhomogeneous due to Euler’s theorem and, as $|Mz| \leq |M| |z|$ for all z , we immediately see that every strongly-subhomogeneous operator is subhomogeneous. However, homogeneity does not necessarily imply strong-subhomogeneity. This is shown for instance in Example 3.2 below. On the other hand, we will see that strong subhomogeneity is preserved under composition while subhomogeneity is not, and this additional property will be useful to establish uniqueness results for brother families of deep equilibrium architectures.

Example 3.2. Let $F : \mathbb{R}^2 \setminus \{[0, 0]\} \rightarrow \mathbb{R}^2$, be defined as $F(z) = F(x, y) = [\frac{x^2 y}{x^2 + y^2}, 0]$. Clearly F is 1-homogeneous, with Jacobian given by

$$F'(z) = \begin{bmatrix} \frac{2xy^3}{(x^2+y^2)^2} & \frac{x^2(x^2-y^2)}{(x^2+y^2)^2} \\ 0 & 0 \end{bmatrix}.$$

Thus, $|F'(z)||z|$ calculated in $z = [1, 2]$ is equal to $[0.56, 0]$, while $F(z) = [0.25, 0]$ in $z = [1, 2]$. This shows that F is not strongly 1-subhomogeneous in \mathbb{R}_{++}^n .

Remark 3.3. Note that subhomogeneity and strong subhomogeneity coincide when the mapping has a positive valued

subgradient. In fact, if $F \in \text{subhom}_\mu(\mathbb{R}_+^n)$ and $\partial F(z) \subseteq \mathbb{R}_+^n$ for all $z \in \mathbb{R}_+^n$, then $|Mz| = Mz = |M||z|$ for all $z \in \Omega$ and all $M \in \partial F(z)$. Thus, $F \in \text{s-subhom}_\mu(\mathbb{R}_+^n)$.

In order to better understand the connection between homogeneity and the two proposed notions of subhomogeneity, we provide below an analogous of Euler's theorem for subhomogeneous operators, directly connecting the notion of subhomogeneous operator with the usual notion of homogeneity $F(\alpha z) = \alpha^\mu F(z)$, see also (Lemmens & Nussbaum, 2012). The proof is moved to Appendix A.

Proposition 3.4. *Let $F : \mathbb{R}^n \rightarrow \mathbb{R}^n$ be differentiable and Lipschitz. Assume moreover that $F(z) > 0$ and $F'(z) > 0$, for all $z > 0$, i.e. the Jacobian $F'(z)$ is an entry-wise strictly positive matrix. Then, for $\mu > 0$, it holds*

$$F \in \text{subhom}_\mu(\mathbb{R}_{++}^n) = \text{s-subhom}_\mu(\mathbb{R}_{++}^n)$$

if and only if for all $\lambda \geq 1$ we have

$$F(\lambda z) \leq \lambda^\mu F(z).$$

Notice that, if F satisfies the hypothesis of Proposition 3.4, then $F(\lambda z) \leq \lambda^\mu F(z)$ for all $\lambda \geq 1$ can be equivalently written as $F(x)\tilde{\lambda}^\mu \leq F(x\tilde{\lambda})$ for all $0 < \tilde{\lambda} \leq 1$, which, for $\mu = 1$ coincides with the definition of subhomogeneity used in e.g. (Lemmens & Nussbaum, 2012).

We provide below our main result showing uniqueness of fixed points for subhomogeneous operators, provided the homogeneity coefficient is small enough. Then, in the next Section 4, we will show that standard feed-forward linear layers of the form $\sigma(Wx)$ with a variety of broadly used activation functions σ are indeed subhomogeneous, sometimes up to a minor modification.

3.1. Main result: Existence and uniqueness of fixed points

In this section, we show that subhomogeneous operators with small enough μ admit a unique fixed point, provided a suitable rescaling is implemented. All proofs are moved to Appendix A.

Consider the cone of positive vectors $\mathbb{R}_{++}^n = \{z \in \mathbb{R}^n : z > 0\}$ and let $\varphi : \mathbb{R}^n \rightarrow \mathbb{R}$ be such that:

- (1-homogeneous) $\varphi(\alpha z) = \alpha \varphi(z)$ for all coefficients $\alpha > 0$;
- (positive) $\varphi(z) > 0$ for each $z > 0$;
- (order-preserving) $\varphi(z) > \varphi(x)$ for each $z > x > 0$.

The proof of the existence and uniqueness of the fixed point is based on the Banach fixed-point theorem and the following fundamental completeness result

Theorem 3.5 (See e.g. (Lemmens & Nussbaum, 2012)). *Let $\varphi : \mathbb{R}^n \rightarrow \mathbb{R}$ be a positive 1-homogeneous function.*

Define the cone slice $\mathbb{R}_{++}^n/\varphi := \{z \in \mathbb{R}_{++}^n : \varphi(z) = 1\}$ and consider the Thomson distance $\delta(x, y) = \|\ln(x) - \ln(y)\|_\infty$. Then, the pair $(\mathbb{R}_{++}^n/\varphi, \delta)$ is a complete metric space.

Based on the theorem above, if we have an operator G that maps $\mathbb{R}_{++}^n/\varphi$ to itself and that is contractive with respect to δ , then G must have a unique fixed point in $\mathbb{R}_{++}^n/\varphi$. Our main theorem below shows that this is always the case when G is defined by rescaling a positive subhomogeneous operator via φ . We start by proving that if G mapping \mathbb{R}_{++}^n to $\mathbb{R}_{++}^m/\varphi$ is defined by rescaling with φ a subhomogeneous operator F , then it is Lipschitz continuous with respect to the Thomson distance, with a Lipschitz constant that depends only on the subhomogeneity degree of F .

Theorem 3.6. *Let $F : \mathbb{R}^n \rightarrow \mathbb{R}^m$ be a Lipschitz operator. Assume that F is positive, i.e. $F(z) > 0$ for all $z > 0$, and that $F \in \text{subhom}_\mu(\mathbb{R}_{++}^n)$ for some $\mu > 0$. For a positive, 1-homogeneous, order-preserving functional $\varphi : \mathbb{R}^m \rightarrow \mathbb{R}$, define the φ -normalization layer map*

$$\text{norm}_\varphi : \mathbb{R}_{++}^n \rightarrow \mathbb{R}_{++}^m/\varphi, \quad \text{norm}_\varphi(z) = z/\varphi(z)$$

and let

$$G(z) = \text{norm}_\varphi(F(z)).$$

Then,

$$\delta(G(x), G(y)) \leq 2\mu \delta(x, y),$$

for all $x, y \in \mathbb{R}_{++}^n$. Moreover, if F is differentiable and that its Jacobian matrix $F'(z)$ is entry-wise positive for all $z \in \mathbb{R}_{++}^n$, then

$$\delta(G(x), G(y)) \leq \mu \delta(x, y),$$

for all $x, y \in \mathbb{R}_{++}^n$.

The following uniqueness result is now a direct consequence of Theorem 3.5 and Theorem 3.6.

Theorem 3.7. *Let $F : \mathbb{R}^n \rightarrow \mathbb{R}^n$, $F \in \text{subhom}_\mu(\mathbb{R}_{++}^n)$, $\varphi : \mathbb{R}^n \rightarrow \mathbb{R}$ be 1-homogeneous, positive, and order-preserving, and let $G = \text{norm}_\varphi \circ F$. If $0 < \mu < 1/2$, then there exists a unique fixed point $G(z^*) = z^* \in \mathbb{R}_{++}^n/\varphi$. Moreover, if F is differentiable and its Jacobian is entry-wise positive for all $z > 0$, then a unique fixed point $z^* \in \mathbb{R}_{++}^n/\varphi$ exists provided $0 < \mu < 1$. In both cases, the sequence $z_{k+1} = G(z_k)$ converges to z with linear convergence rate, namely*

$$\|z_k - z^*\|_\infty \leq C\mu^k,$$

for any $z_0 \in \mathbb{R}_{++}^n$.

It is not difficult to observe that the same conclusion holds if the normalization layer norm_φ is applied in a localized form to different components of the embedding, rather than

as a global scaling factor. This is useful for example when F is matrix-valued, as in the context of graph neural architectures, and one may need to normalize rows or columns of the embedding to e.g. simulate a random walk. See also Section 6.3. We formulate this explicitly for normalization layers acting column-wise in the next corollary, but we underline that its proof (see Appendix A) can be easily adapted to different normalization patterns.

Corollary 3.8. *Let $G : \mathbb{R}^{n \times d} \rightarrow \mathbb{R}^{n \times d}$ be defined as*

$$G(x) = [\text{norm}_{\varphi_1}(F_1(x)), \dots, \text{norm}_{\varphi_d}(F_d(x))],$$

where $F_i : \mathbb{R}^{n \times d} \rightarrow \mathbb{R}^n$ are μ -subhomogeneous and $\varphi_i : \mathbb{R}^n \rightarrow \mathbb{R}$ are 1-homogeneous, positive, order-preserving functions. Then, the same conclusion of Theorem 3.7 holds for G , provided the requirements for F are satisfied by each F_i .

4. Subhomogeneous deep equilibrium models

Consider now the weight-tied, input-injected neural network

$$z^{(k+1)} = \sigma_1(\sigma_2(Wz^{(k)} + f_\theta(x))) \quad (3)$$

in which $x \in \mathbb{R}^d$ denotes the input, $z^{(k)} \in \mathbb{R}^n$ denotes the hidden unit at layer k , $\sigma_1, \sigma_2 : \mathbb{R} \rightarrow \mathbb{R}$ denote activation functions applied entrywise, $W \in \mathbb{R}^{n \times n}$ are the hidden unit weights, $f_\theta : \mathbb{R}^d \rightarrow \mathbb{R}^n$ is an input-injection embedding, e.g. defined by an MLP. We use here a fully connected layer for simplicity, but everything transfers unchanged to the convolutional case (i.e. if Wz is replaced by $W * z$, with W being the convolutional kernel). While in practice using both nonlinearities σ_1 and σ_2 may be redundant, we provide here a theoretical investigation of the model (3) in its generality and we will then study specific architectures where either $\sigma_1 = \text{Id}$ or $\sigma_2 = \text{Id}$.

Theorem 3.7 can be used to show that a unique fixed point for Equation (3) exists, provided we add a final normalization layer:

$$z = \text{norm}_\varphi(\sigma_1(\sigma_2(Wz) + f_\theta(x))) \quad (4)$$

where φ is any positive, 1-homogeneous, order-preserving normalizing function (or multiple functions if the normalization layer is applied locally as in Corollary 3.8). Note that φ can be, for example, any standard p -norm. This type of layer normalization step is also used to e.g. reduce the network sensitivity to small perturbations (Zhang et al., 2022; Farnia et al., 2018) and could accelerate training (Ba et al., 2016; Ioffe & Szegedy, 2015).

To study (4) using Theorem 3.7, we now notice that it is enough to study the subhomogeneity of the activation functions σ_1 and σ_2 . In fact, we can think of $F(z) := \sigma_1(\sigma_2(Wz) + f_\theta(x))$ as the composition of an activation

function σ_1 applied entry-wise, with a translation $T(u) = u + f_\theta(x)$, another activation function σ_2 , and a linear map $L(z) = Wz$ (or $L(z) = W * z$ for convolutional layers),

$$F = \sigma_1 \circ T \circ \sigma_2 \circ L. \quad (5)$$

Linear mappings are particular examples of homogeneous operators while translations are subhomogeneous. In the next lemma, we observe that the subhomogeneity of F coincides with the subhomogeneity of σ_1 and σ_2 , provided the input injection $f_\theta(x)$ is positive (entrywise). This requirement is not excessively restrictive, as it can be satisfied by using a positive nonlinear activation function, such as ReLU, SoftPlus, or by shifting bounded activations such as tanh. All proofs are moved to Appendix A.

Lemma 4.1. *Let Ω be a subset of \mathbb{R}^n , H be h -homogeneous, $P \in \text{subhom}_\mu(H(\Omega))$, T_y denote the translation by y , $T_y(z) = z + y$, and let $\mathbf{Q} \in \text{s-subhom}_\lambda(T_y(P(H(\Omega))))$. Then, if the following composition rules hold:*

- $P \circ H \in \text{subhom}_{h\mu}(\Omega)$
- If $y \geq 0$, then $\mathbf{Q} \circ T_y \circ P \circ H \in \text{subhom}_{h\mu\lambda}(\Omega)$

Thus, studying the subhomogeneity (resp. strong subhomogeneity) of F in (5) boils down to the analysis of the subhomogeneity (resp. strong subhomogeneity) of σ_1 and σ_2 . In particular, note that subhomogeneity is enough for σ_2 while strong homogeneity is required on σ_1 in order for the whole model to be subhomogeneous. However, we notice that in the typical case of activation functions acting entrywise this additional requirement is redundant. In fact, note that these subhomogeneity properties are inherited from the univariate function defining the activation layer when they act entrywise. Precisely, if $\sigma : \mathbb{R} \rightarrow \mathbb{R}$ is a Lipschitz function with $\sigma \in \text{subhom}_\mu(\Omega)$, for $\Omega \subseteq \text{dom}_+(\sigma)$, then we automatically have that the entrywise action of σ on \mathbb{R}^n is $\text{subhom}_\mu(\Omega^n)$, with $\Omega^n = \Omega \times \dots \times \Omega$, as the elements of the Clarke’s generalized Jacobian of σ in $z \in \mathbb{R}^n$ are simply diagonal matrices whose j -th diagonal element is an element of the Clarke’s generalized Jacobian of σ evaluated on the j -th component of z . With the following remark, we can notice that the definitions of subhomogeneous and strongly subhomogeneous coincide in the univariate case.

Remark 4.2. Let $\sigma : \mathbb{R} \rightarrow \mathbb{R}$ be $\sigma \in \text{subhom}_\mu(\Omega)$ for some $\mu > 0$ and some $\Omega \subseteq \mathbb{R}$. Notice that, $|\sigma'(z)z| = |\sigma'(z)||z|$ for each $z \in \Omega$, this implies that $\sigma \in \text{s-subhom}_\mu(\Omega)$.

In the next Section 5 we will show a variety of examples of commonly used activation functions σ that are subhomogeneous. For all such choices, the DEQ model (4) is well-defined as the existence of a unique equilibrium point z is guaranteed.

Subhomogeneous Deep Equilibrium Models

Name	Sigmoid	SoftPlus	Tanh	Tanh + 1.2	Tanh + 1.603	HardTanh	ReLU	Approxmax
μ	1	1	1	0.99	0.499	1	1	1
Ω	\mathbb{R}_+^n	\mathbb{R}_+^n	\mathbb{R}_+^n	\mathbb{R}^n	\mathbb{R}^n	\mathbb{R}^n	\mathbb{R}_{++}^n	\mathbb{R}_+^n
Differentiable	✓	✓	✓	✓	✓			✓

Table 1. Examples of subhomogeneous activation functions

5. Subhomogeneous activation functions

We now propose several examples of subhomogeneous activation functions, they are well-known activation functions commonly used in deep learning. All the proofs are moved to Appendix A.

As a first example, we show that the sigmoid function is subhomogeneous, on the positive real axis, with $\mu = 1$.

Proposition 5.1. *Let $\sigma : \mathbb{R} \rightarrow \mathbb{R}$ be defined as*

$$\sigma(z) = \text{sigmoid}(z) := \frac{e^z}{1 + e^z}.$$

Then $\sigma \in \text{subhom}_1(\mathbb{R}_+)$.

Similarly to the sigmoid, also the SoftPlus is subhomogeneous on \mathbb{R}_+ with $\mu = 1$.

Proposition 5.2. *Let $\sigma : \mathbb{R} \rightarrow \mathbb{R}$ be defined as*

$$\sigma(z) = \text{softplus}(z) := \frac{1}{\beta} \ln(1 + e^{\beta z}),$$

where $\beta > 0$. Then $\sigma \in \text{subhom}_1(\mathbb{R}_+)$.

Other two examples of 1-subhomogeneous operator are the ReLU and the LeakyReLU. While the sigmoid and the SoftPlus are 1-subhomogeneous on \mathbb{R}_+ , the ReLU and the LeakyReLU are 1-subhomogeneous on \mathbb{R}_{++} , this is due to the fact that they are strictly positive only on \mathbb{R}_{++} . As both activation functions are simply the identity on the positive orthant, they clearly are in $\text{subhom}_1(\mathbb{R}_{++})$. This is the case also for the hyperbolic tangent, although being less obvious.

Proposition 5.3. *Let $\sigma : \mathbb{R} \rightarrow \mathbb{R}$ defined as*

$$\sigma(z) = \tanh(z) := \frac{e^z - e^{-z}}{e^z + e^{-z}}.$$

Then, $\sigma \in \text{subhom}_1(\mathbb{R}_+)$.

The examples considered above are activations that are subhomogeneous only on the nonnegative/positive orthant. We provide below an example of subhomogeneous activation function that is subhomogeneous globally. This is obtained as a positive shift of the hyperbolic tangent. In fact, it is not difficult to notice that if $\sigma(z) = \tanh(z) + 1 + \epsilon$ with $\epsilon > 0$, then $\mu(\epsilon) = \max_z |z| \sigma'(z) \sigma(z)^{-1}$ is a decreasing function of ϵ , i.e. $\mu(\epsilon_1) < \mu(\epsilon_2)$ for $\epsilon_1 > \epsilon_2 > 0$. Moreover, it holds $\mu(\epsilon) < 1$ for all

$$\epsilon > 0.199 > \max_z \{ |z| \text{sech}^2(z) - \tanh(z) - 1 \}$$

and $\mu(\epsilon) < 1/2$ for all

$$\epsilon > 0.602 > \max_z \{ 2|z| \text{sech}^2(z) - \tanh(z) - 1 \}.$$

These computations directly lead to

Proposition 5.4. *Let $\sigma : \mathbb{R} \rightarrow \mathbb{R}$ be defined as*

$$\sigma(z) = \tanh(z) + \alpha.$$

If $\alpha > 1$, then $\sigma \in \text{subhom}_\mu(\mathbb{R})$. In particular, if $\alpha > 1.2$ then $\mu < 1$ and if $\alpha > 1.602$ then $\mu < 1/2$.

Finally, similar to the hyperbolic tangent, we notice below that the non-differentiable piece-wise linear hardtanh activation function is 1-subhomogeneous on \mathbb{R} .

Proposition 5.5. *Let $\sigma : \mathbb{R} \rightarrow \mathbb{R}$ be defined as*

$$\sigma(z) = \text{hardtanh}(z) := \begin{cases} \alpha_1 & \text{if } z < \alpha_1 \\ \alpha_2 & \text{if } z > \alpha_2 \\ z & \text{otherwise} \end{cases}$$

with $0 < \alpha_1 < \alpha_2 < \infty$. Then, $\sigma \in \text{subhom}_1(\mathbb{R})$.

All activation functions considered above are univariate functions acting entrywise. Thus they are both subhomogeneous and strongly subhomogeneous as observed in Remark 4.2. In the final example below we consider an example of a subhomogeneous function that is also strongly subhomogeneous but is not pointwise.

Proposition 5.6. *Let $\sigma : \mathbb{R}^n \rightarrow \mathbb{R}$ be defined as*

$$\sigma(z) = \text{Approxmax}(z) = \ln \sum_i e^{z_i} \approx \max_i z_i$$

Then, $\sigma \in \text{subhom}_1(\mathbb{R}_+^n)$ and $\sigma \in \text{s-subhom}_1(\mathbb{R}_+^n)$.

The power scaling trick

Theorem 3.7 ensures a unique fixed point for any subhomogeneous operator F exists, provided the subhomogeneity degree is small enough. As we have shown with the examples above, subhomogeneity is not a very stringent requirement, and many operators commonly used in deep learning are actually subhomogeneous without any modification. However, it is often the case that $\mu \geq 1$. To reduce the degree of \tanh , we applied a positive shift α . However, applying

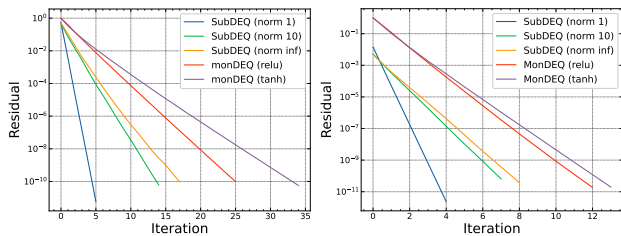


Figure 1. Iteration required by the fixed point method for dense SubDEQ vs Peaceman-Rachford method for dense MonDEQ. Left: linear layer; Right: convolutional layer.

a scalar shift might not work all the time. When the subhomogeneity constant is not small enough, a simple ‘‘power scaling trick’’ can be implemented for any subhomogeneous F . In fact, it follows directly from Lemma 4.1 that if F is μ -subhomogeneous, then F^α defined as the entrywise power $F^\alpha(x) = F(x)^\alpha$, is $\alpha\mu$ -subhomogeneous, since the map $x \mapsto x^\alpha$ is strongly α -subhomogeneous. Thus, to ensure uniqueness for (4) when σ_i are 1-subhomogeneous, we can mildly perturb σ_i into $\tilde{\sigma}_i(x) = \sigma_i(x)^{1-\varepsilon}$, for any $\varepsilon > 0$ arbitrary small. With this perturbed activation the DEQ in (4) is guaranteed to have a unique fixed point.

6. Experiments

We illustrate the performance of DEQ networks as in Equation (4) on benchmark image datasets, as compared to alternative standard implicit neural networks, precisely Monotone operator-based DEQ (MonDEQ) (Winston & Kolter, 2020) and neural ordinary differential equations (nODE) (Chen et al., 2018). As discussed in Section 4, we will use only one σ_i different from the identity function. To this end, with we first consider the case $\sigma_1 = \text{Id}$, that is

$$z = \text{norm}_\varphi(\sigma(Wz) + f_\theta(x)).$$

Thanks to Theorem 3.7 and Lemma 4.1 we can choose a suitable activation function σ to guarantee the subhomogeneity of the architecture and thus the existence and uniqueness of the fixed point z . Here we experiment with $\sigma(z) = \tanh(z) + \alpha$, with $\alpha = 1.603$ chosen accordingly to Proposition 5.4. This ensures a small enough subhomogeneity degree ($\mu < 1/2$) and thus uniqueness by Theorem 3.7. Precisely, we let

$$z = \text{norm}_{\|\cdot\|_p}(\tanh(Wz) + f_\theta(x) + 1.603), \quad (6)$$

where $1 \leq p \leq +\infty$ and $f_\theta(x)$ is a one-layer MLP with entry-wise positive final activation layer. As the architecture is now subhomogeneous and has a unique fixed point, we call (6) a SubDEQ.

6.1. Efficiency of SubDEQ

We now compare the convergence rate of the standard fixed-point method to find the equilibrium point of a SubDEQ, which is globally convergent due to Theorem 3.7, with the convergence rate of the Peaceman-Rachford method to find the equilibrium point of a MonDEQ (Winston & Kolter, 2020). We analyze the implicit-layer of the SubDEQ in (6) varying $p \in \{1, 10, +\infty\}$ and letting $f_\theta(x) = \text{ReLU}(Ux + b)$ be a one-layer MLP with ReLU activation function. We implement two different MonDEQs: the first one is defined as in (Winston & Kolter, 2020) via the following equation

$$z = \text{ReLU}(Wz + Ux + b). \quad (7)$$

The second one is defined as

$$z = \tanh(Wz + f_\theta(x)). \quad (8)$$

to replicate the architecture of the proposed SubDEQ.

In order to guarantee that the MonDEQ architectures have a unique fixed point, we restrict the weight matrix W in both the MonDEQ equations to satisfy the operator monotone parametrization

$$W = A^\top A + B - B^\top$$

with A, B parameter matrices, c.f. (Winston & Kolter, 2020).

For all models, as input, we choose $x \in \mathbb{R}^{128 \times 400}$ sampled from a uniform distribution on the interval $[0, 1)$ using `torch.rand`, the first dimension represents the batch-size and the second the dimension of the features space. The hidden embedding z has a width of 150.

In Figure 1 we plot the relative residual

$$\|z_{k+1} - z_k\|_F / \|z_{k+1}\|_F,$$

where $\|\cdot\|_F$ is the Frobenius norm and z_k are the iterates of the fixed point methods. From Figure 1(left) we can notice that SubDEQ systematically requires less amount of steps to converge with respect to MonDEQ. We also compare with the case of convolutional layers, instead of dense DEQ layers. In this setting, the input $x \in \mathbb{R}^{128 \times 1 \times 28 \times 28}$ is sampled from a uniform distribution on the interval $[0, 1)$ using `torch.rand`, the first dimension represent the batch-size, the second the number of the image channels and the last two the size of the image. The hidden fixed point embedding z has 40 channels and each channel has a size of 28×28 . The relative residual of the iterations is shown in Figure 1(right). Also in this case, we can notice that SubDEQ systematically requires less amount of steps to converge than MonDEQ.

6.2. SubDEQ on benchmark image datasets

We now show the capacity of SubDEQ in terms of classification tasks. We train them on different image benchmark

Model	Error %
MNIST (Dense)	
SubDEQ (ShiftedTanh)	2.088 ± 0.1405 %
SubDEQ (Tanh)	2.174 ± 0.0595 %
nODE (ReLU)	2.784 ± 0.1102 %
nODE (Tanh)	4.046 ± 0.3327 %
MonDEQ (ReLU)	2.18 ± 0.1178 %
MonDEQ (Tanh)	2.556 ± 0.1578 %
MNIST (Convolutional)	
SubDEQ (ShiftedTanh)	1.354 ± 0.98 %
SubDEQ (Tanh)	1.02 ± 0.0642 %
nODE (ReLU)	1.456 ± 0.1278 %
nODE (ReLU)	1.168 ± 0.0823 %
MonDEQ (ReLU)	0.948 ± 0.057 %
MonDEQ (Tanh)	1.122 ± 0.07 %
CIFAR-10	
SubDEQ (ShiftedTanh)	28.364 ± 0.377 %
SubDEQ (Tanh)	28.166 ± 0.6568 %
nODE (ReLU)	33.89 ± 0.483 %
nODE (ReLU)	33.14 ± 0.6099 %
MonDEQ (ReLU)	26.218 ± 0.3069 %
MonDEQ (Tanh)	28.16 ± 0.3069 %
SVHN	
SubDEQ (ShiftedTanh)	9.3562 ± 0.2122 %
SubDEQ (Tanh)	9.9539 ± 0.5556 %
nODE (ReLU)	26.5181 ± 4.1807 %
nODE (Tanh)	17.0206 ± 0.4673 %
MonDEQ (ReLU)	11.0356 ± 0.319 %
MonDEQ (Tanh)	13.3904 ± 3696 %

Table 2. Mean ± std of the misclassification error on test set

datasets: CIFAR-10 (Krizhevsky & Hinton, 2009), SVHN (Netzer et al., 2011), and MNIST (LeCun & Cortes, 2010). We compare SubDEQ with MonDEQ as well as neural ode (nODE) architectures (Chen et al., 2018). Overall, we consider the following models (for the feedforward implicit layer case):

1. SubDEQ (shiftedtanh): $\text{norm}_{\|\cdot\|_\infty}(\tanh(Wz) + f_\theta(x) + 1.603)$
2. SubDEQ (tanh): $\text{norm}_{\|\cdot\|_\infty}(\tanh(Wz) + f_\theta(x))$
3. MonDEQ (ReLU): $z = \text{ReLU}(Wz + Ux + b)$
4. MonDEQ (tanh): $z = \tanh(Wz + f_\theta(x))$
5. nODE (ReLU): $\dot{z}(t) = \text{ReLU}(Wz(t)), z(0) = f_\theta(x)$
6. nODE (tanh): $\dot{z}(t) = \tanh(Wz(t)), z(0) = f_\theta(x)$.

We consider also a convolutional variant of these implicit-layers, the only difference with the above dense layers is in the weights matrices, which we substitute with the standard convolutional kernels. For the SubDEQ, we decide to normalize each element of the batch for the feedforward, while with the convolutions we normalize along each row. For the nODE, we integrate the ODE over the interval $[0, 1]$, as the

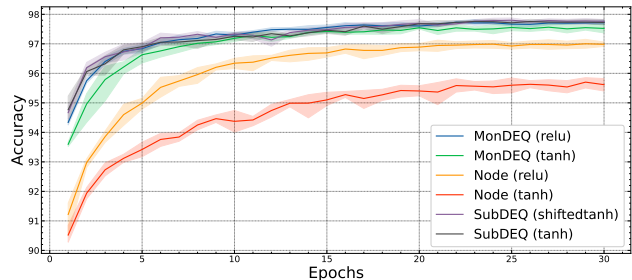


Figure 2. Validation accuracy of the dense architectures during training on MNIST.

output of the implicit layer we took the solution at time $t = 1$. To have a fairer comparison among the models, we normalize the output of the implicit-layers of the MonDEQ and the nODE using the same norm as the SubDEQ. For all the models, in order to mitigate the normalization effect, on the normalized output of the implicit layers, we apply 1d batch normalization for the feedforward layers and 2d batch normalization for the convolutional layers. Moreover, as a last step, we feed the embedding into a softmax classifier, but with the convolutional architectures, before it, we apply an average pooling and then we flatten the tensor. We describe all the details about the hyperparameters in Table 5 in Appendix B.

For every experiment, with the SubDEQ architectures, we use the fixed point method sped up with Anderson acceleration to calculate the fixed point and as the stopping criterion we use the relative residual

$$\|z_{k+1} - z_k\|_F / \|z_{k+1}\|_F,$$

and we stop the method when the residual reaches the values of 10^{-3} . We decided to train the dense architecture only on MNIST, instead, we trained the convolutional models on all three data sets. Regarding the data, we use the hold-out approach, dividing the dataset into train validation and test sets. Table 4 describes the proportion of the splittings. All training data is normalized to mean $\mu = 0$, standard deviation $\sigma = 1$, and the validation and the test are rescaled using the mean and standard deviation of the training data. On the same data split we run the experiments 5 times and in Section 6.2 we show the mean ± the standard deviation of the misclassification error. As we can notice from Section 6.2, the SubDEQ (shiftedtanh), depending on the dataset, achieves performance that exceeds the performance of the other model or reaches similar performance to the best model. We highlight that adding the vector 1.603 to the activation function to ensure the uniqueness and convergence, does not negatively affect the performance, instead ensures higher stability and leads the model to a higher accuracy.

Dataset (% labeled)	Accuracy
Cora citation (5.2 %)	
APPNP	80.2027 ± 1.9557 %
APPNP (ShiftedTanh)	73.3905 ± 2.3818 %
Cora author (5.2 %)	
APPNP	70.834 ± 2.1591 %
APPNP (ShiftedTanh)	73.3437 ± 1.8252 %
CiteSeer (4.2 %)	
APPNP	62.8625 ± 1.4477 %
APPNP (ShiftedTanh)	62.66078 ± 1.8676 %
DBLP (4.0 %)	
APPNP	88.8095 ± 0.2866
APPNP (ShiftedTanh)	89.4007 ± 0.3619 %
PubMed (0.8 %)	
APPNP	77.4967 ± 1.4522 %
APPNP (ShiftedTanh)	78.5827 ± 0.9741 %

Table 3. Mean ± standard deviation accuracy on test set

6.3. Deep Equilibrium Graph Neural Network: nonlinear graph propagation

We conclude with an experiment on a graph neural network architecture. Graph neural networks are typically relatively shallow due to oversmoothing and oversquashing phenomena (Nguyen et al., 2023; Giraldo et al., 2023). Thus, a fixed point implicit graph neural architecture may be ineffective. However, it is shown in (Gasteiger et al., 2022) that the PageRank random walk on the graph may be used to propagate the input injected by a simple MLP and the limit point of the propagation leads to excellent, sometimes state-of-the-art, results. This approach, named there APPNP, is effective also because the PageRank diffusion process converges linearly to a unique PageRank vector. As the model uses the PageRank fixed point as the final latent embedding, it can be interpreted as a simple DEQ with linear activations. This is possibly a limitation of APPNP as nonlinear activations may allow for a better modeling power. Using Theorem 3.7 one can propose variations of this approach implementing nonlinear diffusion processes based on subhomogeneous activation functions and still maintain the same fundamental guarantees of uniqueness and linear convergence. We obtain this way a SubDEQ variation of the APPNP graph neural network model, which we discuss next.

First, we review the standard APPNP architecture (Gasteiger et al., 2022). Consider an undirected graph $G = (V, E)$ on $n = |V|$ nodes, let d_i be the degree of node i , and let A be the graph normalized adjacency matrix, defined as $A_{ij} = d_i$ if $ij \in E$ and $A_{ij} = 0$ otherwise. APPNP defines the node embedding Z via the fixed point equation:

$$\begin{cases} \tilde{Z} = (1 - \alpha)\tilde{A}\tilde{Z} + \alpha f_\theta(X) \\ Z = \text{softmax}(\tilde{Z}) \end{cases} \quad (9)$$

where $\tilde{A} = A + I$ denotes the shifted adjacency matrix and $X \in \mathbb{R}^{n \times f}$ is the input node feature matrix.

We consider here the following nonlinear variation of (9)

$$\begin{cases} \tilde{Z} = \text{norm}_{\|\cdot\|_\infty} \left(\tanh((1 - \alpha)\tilde{A}\tilde{Z}) + \alpha f_\theta(X) + 1.2 \right) \\ Z = \text{softmax}(\tilde{Z}) \end{cases}$$

where the final normalization layer is implemented column-wise, as in Corollary 3.8.

If we add to \tanh a translation vector with all entries equal to 1.2, we obtain a subhomogeneous operator with degree $\mu = 0.99$, due to the Proposition 5.4 and Lemma 4.1. Notice also that the Jacobian with respect Z of this transformation is entrywise positive respect all $Z > 0$ and is differentiable, then the nonlinear fixed point equation above has a unique fixed point due to Corollary 3.8. We test APPNP and its nonlinear variation on different graph datasets: Cora citation, Cora author, CiteSeer, DBLP, and PubMed, always in a node classification semi-supervised learning setting. We divide the dataset into training, validation, and test sets. The percentages of observation used for the training set are shown in Table 6.3, and the remaining observations are equally split between validation and test sets. For both methods, we use similar hyperparameters, as $f_\theta(\cdot)$ we use 2-layers MLP of width 64 for each layer; we regularize the architectures with dropout $p = 0.5$, we use Adam as optimizer with constant learning rate equal to 0.01 and a weight decay equal to 0.005. We set $\alpha = 0.1$ and $K = 10$. We repeat the splitting and the training 5 times and we report the average ± std results in table 6.3.

7. Conclusions

We have introduced a new class of implicit-depth neural networks that are provably well defined in the sense that they are guaranteed to have a unique fixed point, which we can compute via a fast converging fixed point iteration. Unlike previous approaches that require constraints on the weight matrices to guarantee uniqueness, our theoretical framework allows us to use general weight matrices, provided the activation functions of the network are subhomogeneous and a final normalization layer is added to the architecture. We observe that many well-known activation functions are indeed subhomogeneous possibly up to some minor modification. Thus, we provide several examples of new subhomogeneous deep equilibrium architectures designed for image classification and nonlinear graph propagation.

References

- Ba, J. L., Kiros, J. R., and Hinton, G. E. Layer normalization, 2016.
- Bai, S., Kolter, J. Z., and Koltun, V. Neural ordinary differen-

- tial equations. *Advances in neural information processing systems*, 32:688–699, 2019.
- Bai, S., Koltun, V., and Kolter, J. Z. Multiscale deep equilibrium models, 2020.
- Bai, S., Geng, Z., Savani, Y., and Kolter, J. Z. Deep equilibrium optical flow estimation, 2022.
- Chen, Q., Wang, Y., Geng, Z., Wang, Y., Yang, J., and Lin, Z. Equilibrium image denoising with implicit differentiation. *IEEE Transactions on Image Processing*, 32:1868–1881, 2023. doi: 10.1109/TIP.2023.3255104.
- Chen, R. T. Q., Rubanova, Y., Bettencourt, J., and Duvenaud, D. Neural ordinary differential equations. *Advances in neural information processing systems*, 31:6571–6583, 2018.
- Chen, T., Lasserre, J.-B., Magron, V., and Pauwels, E. Semi-algebraic representation of monotone deep equilibrium models and applications to certification, 2021.
- Clarke, F. H. *Optimization and Nonsmooth Analysis*. Society for Industrial and Applied Mathematics, 1990. doi: 10.1137/1.9781611971309. URL <https://epubs.siam.org/doi/abs/10.1137/1.9781611971309>.
- Dabre, R. and Fujita, A. Recurrent stacking of layers for compact neural machine translation models. In *Proceedings of the AAAI Conference on Artificial Intelligence*, volume 33, pp. 6292–6299, 2019.
- Dehghani, M., Gouws, S., Vinyals, O., Uszkoreit, J., and Kaiser, L. Universal transformers. In *International Conference on Learning Representations (ICLR)*, 2019.
- Farnia, F., Zhang, J. M., and Tse, D. Generalizable adversarial training via spectral normalization, 2018.
- Gasteiger, J., Bojchevski, A., and Günnemann, S. Predict then propagate: Graph neural networks meet personalized pagerank, 2022.
- Gautier, A., Tudisco, F., and Hein, M. The perron–frobenius theorem for multihomogeneous mappings. *SIAM Journal on Matrix Analysis and Applications*, 40(3):1179–1205, 2019.
- Ghaoui, L. E., Gu, F., Travacca, B., Askari, A., and Tsai, A. Y. Implicit deep learning, 2020.
- Gilton, D., Ongie, G., and Willett, R. Deep equilibrium architectures for inverse problems in imaging, 2021.
- Giraldo, J. H., Skianis, K., Bouwmans, T., and Malliaros, F. D. On the trade-off between over-smoothing and over-squashing in deep graph neural networks. In *Proceedings of the 32nd ACM International Conference on Information and Knowledge Management, CIKM '23*. ACM, October 2023. doi: 10.1145/3583780.3614997. URL <http://dx.doi.org/10.1145/3583780.3614997>.
- Gu, F., Chang, H., Zhu, W., Sojoudi, S., and Ghaoui, L. E. Implicit graph neural networks, 2021.
- Ioffe, S. and Szegedy, C. Batch normalization: Accelerating deep network training by reducing internal covariate shift, 2015.
- Jafarpour, S., Davydov, A., Proskurnikov, A. V., and Bullo, F. Robust implicit networks via non-euclidean contractions, 2022.
- Krizhevsky, A. and Hinton, G. Learning multiple layers of features from tiny images. Technical Report 0, University of Toronto, Toronto, Ontario, 2009. URL <https://www.cs.toronto.edu/~kriz/learning-features-2009-TR.pdf>.
- LeCun, Y. and Cortes, C. MNIST handwritten digit database. 2010. URL <http://yann.lecun.com/exdb/mnist/>.
- Lemmens, B. and Nussbaum, R. *Nonlinear Perron–Frobenius Theory*. Cambridge Tracts in Mathematics. Cambridge University Press, 2012. doi: 10.1017/CBO9781139026079.
- Micaelli, P., Vahdat, A., Yin, H., Kautz, J., and Molchanov, P. Recurrence without recurrence: Stable video landmark detection with deep equilibrium models, 2023.
- Netzer, Y., Wang, T., Coates, A., Bissacco, A., Wu, B., and Ng, A. Y. Reading digits in natural images with unsupervised feature learning. In *NIPS Workshop on Deep Learning and Unsupervised Feature Learning 2011*, 2011. URL http://ufldl.stanford.edu/housenumbers/nips2011_housenumbers.pdf.
- Nguyen, K., Nong, H., Nguyen, V., Ho, N., Osher, S., and Nguyen, T. Revisiting over-smoothing and over-squashing using ollivier-ricci curvature, 2023.
- Pokle, A., Geng, Z., and Kolter, Z. Deep equilibrium approaches to diffusion models, 2022.
- Rusch, T. K. and Mishra, S. Coupled oscillatory recurrent neural network (cornn): An accurate and (gradient) stable architecture for learning long time dependencies. In *International Conference on Learning Representations*, 2021.
- Ryu, E. K. and Boyd, S. Primer on monotone operator methods. *Appl. comput. math*, 15(1):3–43, 2016.

- Wei, C. and Kolter, J. Z. Certified robustness for deep equilibrium models via interval bound propagation. In *International Conference on Learning Representations*, 2022. URL <https://openreview.net/forum?id=y1PXylgrXZ>.
- Winston, E. and Kolter, J. Z. Monotone operator equilibrium networks. *Advances in neural information processing systems*, 33:10718–10728, 2020.
- Yang, Z., Pang, T., and Liu, Y. A closer look at the adversarial robustness of deep equilibrium models. In Koyejo, S., Mohamed, S., Agarwal, A., Belgrave, D., Cho, K., and Oh, A. (eds.), *Advances in Neural Information Processing Systems*, volume 35, pp. 10448–10461. Curran Associates, Inc., 2022. URL https://proceedings.neurips.cc/paper_files/paper/2022/file/43da8cca8f14139774bcbd935d51e0f2-Paper-Conference.pdf.
- Zhang, B., Jiang, D., He, D., and Wang, L. Rethinking lipschitz neural networks and certified robustness: A boolean function perspective, 2022.
- Zhao, Y., Zheng, S., and Yuan, X. Deep equilibrium models for video snapshot compressive imaging, 2023.

A. Proofs

Proof. (Proposition 3.4)
Necessary condition.

Let $g: [1, +\infty) \rightarrow \mathbb{R}^n$, defined as

$$g(\lambda) = [g_1(\lambda), \dots, g_n(\lambda)] = F(\lambda z) - \lambda^\mu F(z)$$

Clearly, $g(1) = 0$ and g is a differentiable function since $F(z) > 0$ for each $z > 0$ and F is differentiable.

$$\begin{aligned} g'(\lambda) &= F'(\lambda z)z - \mu\lambda^{\mu-1}F(z) \\ \lambda g'(\lambda) &= F'(\lambda z)\lambda z - \mu\lambda^\mu F(z). \end{aligned}$$

Using the definition of subhomogeneous operator we get

$$\lambda g'(\lambda) \leq \mu(F(\lambda z) - \lambda^\mu F(z)) = \mu g(\lambda).$$

Then $g'_j(\lambda) \leq \frac{\mu}{\lambda} g_j(\lambda)$ for each $j = 1, \dots, n$, thanks to the Grönwall's inequality,

$$g'_j(\lambda) \leq g_j(1)\mu \int_1^\lambda \frac{1}{t} dt = g_j(1)\ln(\lambda) = 0.$$

Therefore, $g'_j(\lambda) \leq 0$, this shows that g_j is a decreasing function and $g_j(\lambda) \leq 0$, thus $g(\lambda) \leq 0$ entry-wise.
Sufficient condition.

Let $g: [0, +\infty) \rightarrow \mathbb{R}^n$ be defined as $g(\lambda) = F(\lambda z) - \lambda^\mu F(z)$, by hypothesis, for each $\lambda \geq 1$, $g(\lambda) \leq 0$, also note that $g(1) = 0$. This shows that $g'(\lambda) \leq 0$ for each $\lambda \geq 1$.

$$g'(\lambda) = F'(\lambda z)z - \mu\lambda^{\mu-1}F(z).$$

We get

$$g'(1) = F'(z)z - \mu F(z),$$

which implies $F'(z)z \leq \mu F(z)$. □

Proof. (Theorem 3.6)

For the Euler's Homogeneous Function Theorem $\varphi(z) = w_z^\top z$, thus $G(z) = \frac{F(z)}{w_z^\top F(z)}$. Let $D(z)$ be Clark's generalized Jacobian of the map $z \rightarrow \ln(G(e^z))$. For the Mean Theorem (Clarke, 1990) we have

$$\ln(G(e^{\ln(x)})) - \ln(G(e^{\ln(y)})) \in \text{co}(D(\Omega(x, y))(\ln(x) - \ln(y))),$$

where $\Omega(x, y) := \{z \in \mathbb{R}^n \mid z = t\ln(x) + (1-t)\ln(y), t \in [0, 1]\}$ and $\text{co}(D(\Omega(x, y))(\ln(x) - \ln(y)))$ denotes the convex hull of all points of the form $Z(\ln(x) - \ln(y))$ where $Z \in D(u)$ for some u in $\Omega(x, y)$.

For the Caratheodory Theorem, we get

$$\ln(G(e^{\ln(x)})) - \ln(G(e^{\ln(y)})) = \sum_{j=0}^{nm} \beta_j \xi_j (\ln(x) - \ln(y)).$$

where $\xi_j \in D(u)$ for a u in $\Omega(x, y)$, $\beta_j \geq 0$ and $\sum_i \beta_i = 1$. For simplicity we will pose $v = \ln(x) - \ln(y)$. Using the Chain Rule (Clarke, 1990) we obtain

$$D(u)v \subseteq (\text{Diag}(G(e^u))^{-1} \partial G(e^u) \text{Diag}(e^u)) v,$$

$\partial G(u)$ denotes the Clark's Generalized Jacobian of G with respect u . Since $G(x) = \frac{F(x)}{w_x^\top F(x)}$ if we apply the chain rule (Clarke, 1990) several times we obtain

$$\partial G(e^u) \text{Diag}(e^u) v \subseteq \left(\frac{\partial F(e^u)}{w_u^\top F(e^u)} - \frac{F(e^u)w_u^\top \partial F(e^u)}{(w_u^\top F(e^u))^2} \right) \text{Diag}(e^u) v,$$

the right-hand side above denote the set of points $Q \text{Diag}(e^u) v$ where $Q = \frac{H}{w_u^\top F(e^u)} - \frac{F(e^u)w_u^\top K}{(w_u^\top F(e^u))^2}$ and $H, K, \in \partial F(e^u)$. Therefore we can write the element of $D(u)v$ as

$$\text{Diag}(G(e^u))^{-1}Q \text{Diag}(e^u)v.$$

At this point, we will estimate $\delta(G(x), G(y))$ using the calculations that we have done so far.

$$\begin{aligned} \delta(G(x), G(y)) &= \|\ln(G(x)) - \ln(G(y))\|_\infty = \left\| \sum_{j=0}^{mn} \beta_j \xi_j (\ln(x) - \ln(y)) \right\|_\infty \leq \\ &\leq \sum_{j=0}^{mn} \beta_j \|\xi_j\|_\infty \|\ln(x) - \ln(y)\|_\infty \leq \max_{j=0, \dots, mn} \|\xi_j\|_\infty \|\ln(x) - \ln(y)\|_\infty. \end{aligned} \quad (10)$$

Now we estimate the infinity norm of a matrix of the form $\text{Diag}(G(e^u))^{-1}Q \text{Diag}(e^u)$. Let us begin by focusing on the first two matrices of multiplication, thus

$$\begin{aligned} \text{Diag}(G(e^u))^{-1}Q &= \text{Diag}(F(e^u))^{-1}w_u^\top F(e^u)Q = \\ &= \text{Diag}(F(e^u))^{-1}H - \frac{\mathbf{1}w_u^\top K}{w_u^\top F(e^u)}, \end{aligned}$$

consequently, the entries are

$$\begin{aligned} |\text{Diag}(G(e^u))^{-1}Q|_{ij} &= \left| \text{Diag}(F(e^u))^{-1}H - \frac{\mathbf{1}w_u^\top K}{w_u^\top F(e^u)} \right|_{ij} = \left| \frac{H_{ij}}{f(e^u)_i} - \sum_{l=1}^m \frac{w_{u,l}K_{lj}}{\sum_r w_{u,r}F(e^u)_r} \right| = \\ &= \left| \frac{H_{ij}}{F(e^u)_i} - \sum_{l=1}^m \frac{w_{u,l}F(e^u)_l}{\sum_r w_{u,r}F(e^u)_r} \frac{K_{lj}}{F(e^u)_l} \right| = \left| \frac{H_{ij}}{F(e^u)_i} - \sum_{l=1}^m \gamma_l \frac{K_{lj}}{F(e^u)_l} \right|, \end{aligned}$$

where $\gamma_i = \frac{w_{u,i}F(e^u)_i}{\sum_r w_{u,r}F(e^u)_r}$. Notice that γ_i are positive and $\sum_i \gamma_i = 1$, thus

$$\begin{aligned} \|\text{Diag}(G(e^u))^{-1}Q \text{Diag}(e^u)\|_\infty &= \max_{i=1, \dots, m} \sum_{j=1}^n |\text{Diag}(G(e^u))^{-1}Q \text{Diag}(e^u)|_{ij} = \\ &= \max_{i=1, \dots, m} \sum_{j=1}^n \left| \frac{H_{ij}e_j^u}{F(e^u)_i} - \sum_{l=1}^m \gamma_l \frac{K_{lj}e_j^u}{F(e^u)_i} \right| \leq \\ &\leq \max_{i=1, \dots, m} \left| \frac{(He^u)_i}{F(e^u)_i} \right| + \max_{i=1, \dots, m} \left| \frac{(Ke^u)_i}{F(e^u)_i} \right| \leq \mu + \mu = 2\mu. \end{aligned} \quad (11)$$

Finally we obtain $\max_{j=0, \dots, mn} \|\xi_j\|_\infty \leq 2\mu$, that conclude the proof of the first part. We now assume that F is differentiable and its Jacobian is entrywise positive for each $z > 0$. Until Equation (10) the proof is the same as the first part. Therefore, we can start estimating $\text{Diag}(G(e^u))^{-1}Q \text{Diag}(e^u)$ as following

$$\begin{aligned} |\text{Diag}(G(e^u))^{-1}Q|_{ij} &= \left| \text{Diag}(F(e^u))^{-1}J_F(e^u) - \frac{\mathbf{1}w_u^\top J_F(e^u)}{w_u^\top F(e^u)} \right|_{ij} = \left| \frac{J_F(e^u)_{ij}}{F(e^u)_i} - \sum_{l=1}^m \frac{w_{u,l}J_F(e^u)_{lj}}{\sum_r w_{u,r}F(e^u)_r} \right| = \\ &= \left| \frac{J_F(e^u)_{ij}}{F(e^u)_i} - \sum_{l=1}^m \frac{w_{u,l}F(e^u)_l}{\sum_r w_{u,r}F(e^u)_r} \frac{J_F(e^u)_{lj}}{F(e^u)_l} \right| =: \left| C_{ij} - \sum_{l=1}^m \gamma_l C_{lj} \right| \end{aligned}$$

where $\gamma_i = \frac{w_{u,i}F(e^u)_i}{\sum_r w_{u,r}F(e^u)_r}$ and $C_{ij} = \frac{J_F(e^u)_{ij}}{F(e^u)_i}$. Notice that γ_i and C_{ij} are positive and $\sum_i \gamma_i = 1$.

$$|C_{ij} - \sum_{l=1}^m \gamma_l C_{lj}| \leq \max_{l=1, \dots, m} C_{lj} =: C_{ij}.$$

Thus

$$\begin{aligned} \|\text{Diag}(G(e^u))^{-1}Q\text{Diag}(e^u)\|_\infty &= \max_{i=1,\dots,m} \sum_{j=1}^n |\text{Diag}(G(e^u))^{-1}Q\text{Diag}(e^u)|_{ij} = \\ &= \max_{i=1,\dots,m} \sum_{j=1}^n |\text{Diag}(G(e^u))^{-1}Q|_{ij} e_j^u \leq \\ &\leq \sum_{j=1}^n C_{\bar{l}j} e_j^u = \sum_{j=1}^n \frac{J_F(e^u)_{\bar{l}j}}{F(e^u)_{\bar{l}}} e_j^u \leq \mu \end{aligned}$$

which concludes the proof. \square

Proof. (Corollary 3.8)

Let

$$\delta(G(x), G(y)) = \max_{\substack{i=1,\dots,n \\ j=1,\dots,d}} |\ln(x_{ij}) - \ln(y_{ij})|$$

be the Thompson distance on $\mathbb{R}^{n \times d}$. Let $G_j : \mathbb{R}^{n \times d} \rightarrow \mathbb{R}^n$ be the j -th column mapping of G .

$$\delta(G(x), G(y)) = \max_{\substack{i=1,\dots,n \\ j=1,\dots,d}} |\ln(x_{ij}) - \ln(y_{ij})| = \max_{j=1,\dots,d} \left(\max_{i=1,\dots,n} |\ln(x_{ij}) - \ln(y_{ij})| \right) = \max_{j=1,\dots,d} \delta(G_j(x), G_j(y)).$$

Applying Theorem 3.6 with input space $\mathbb{R}^{n \times d}$ and output space \mathbb{R}^n , we obtain

$$\delta(G_j(x), G_j(y)) \leq 2\mu\delta(x, y)$$

for all $j = 1, \dots, d$. Thus

$$\max_{j=1,\dots,d} \delta(G_j(x), G_j(y)) \leq 2\mu\delta(x, y).$$

This concludes the proof of the first part. Applying the same argument one can prove the case of positive Jacobian yielding the same upper bound without 2. \square

Proof. (Lemma 4.1)

Now we start proving the first part, hence that $P \circ H$ is $h\mu$ -subhomogeneous. Using the chain rule we obtain $\partial(P \circ H)(z)z = \partial P(H(z))J_H(z)z$, where $\partial(P \circ H)(z)$ and $\partial P(H(z))$ are the Clarke's generalized Jacobians of P and $P \circ H$, respectively evaluated in z and $P(z)$, and $J_H(z)$ is the Jacobian of H in z .

Therefore we can write an element of $\partial(P \circ H)(z)z$ as $MJ_H(z)z$, with $M \in \partial P(z)$. Moreover, applying Euler's Homogeneous Function Theorem and the definition of subhomogeneity we get

$$|MJ_H(z)z| = h|M_H(z)| \leq h\mu P(H(z)) = h\mu(P \circ H)(z).$$

Thus, $P \circ H \in \text{subhom}_{h\mu}$.

We now prove the second part of the Lemma, hence $Q \circ T_y \circ P \circ H$ is $h\mu\lambda$ -subhomogeneous. Let $F = Q \circ T_y \circ P \circ H$ and $\mathbf{P} = P \circ H$, for the first point is $h\mu$ -subhomogeneous. let $\partial F(z)z \subseteq \text{co}\{\partial Q(\mathbf{P}(z) + y)\partial \mathbf{P}(z)\}z$. Thus, an element $M \in \partial F(z)$ can be written as

$$Mz = \sum_{k=0}^n \beta_k M_k^Q M_k^P z,$$

where $\beta_k \geq 0$ and $\sum_k \beta_k = 1$, $M_k^Q \in \partial Q(\mathbf{P}(z) + y)$ and $M_k^P \in \partial \mathbf{P}(z)$. We get

$$|Mz| = \left| \sum_{k=0}^n \beta_k M_k^Q M_k^P z \right| \leq \lambda \sum_{k=0}^n \beta_k |M_k^Q| |\mathbf{P}(z)| \leq \lambda \sum_{k=0}^n \beta_k |M_k^Q| (\mathbf{P}(z) + y) \leq \lambda \mu Q(\mathbf{P}(z) + y) = \lambda \mu F(z).$$

Therefore, $Q \circ T_y \circ P \circ H \in \text{subhom}_{h\mu\lambda}$. \square

Proof. (Proposition 5.1)

If $z \geq 0$, $\sigma(z) > 0$, then $\mathbb{R}_+ \subseteq \text{dom}_+(\sigma)$. Also note that

$$\sigma'(z) = \frac{e^z(1+e^z) - e^z e^z}{(1+e^z)^2} = \sigma(z)(1-\sigma(z)).$$

Since $\sigma(z) = \frac{e^z}{1+e^z}$, the inequality that we want to prove is equivalent to $z \leq 1+e^z$. In 0 the inequality is verified, moreover, if we calculate the derivative of both sides we obtain

$$1 \leq e^z,$$

$e^0 = 1$ and e^z is a monotone increasing function, thus the inequality is verified. Therefore $\sigma \in \text{subhom}_1(\mathbb{R}_+)$. □

Proof. (Proposition 5.2)

If $z \geq 0$, $p(z) > 0$, thus $\mathbb{R}_+ \subseteq \text{dom}_+(p)$.

$$p'(z) = \frac{e^{\beta z}}{1+e^{\beta z}},$$

$0 < p'(z) < 1$, thus p is a monotonic increasing function. Therefore what we want to show coincides with

$$p'(z)x \leq p(z).$$

Moreover, $p'(z)z \leq x$, since $0 < p'(z) < 1$. Clearly is enough to proof $\beta z \leq \ln(1+e^{\beta z})$, this is equivalent to $e^{\beta z} \leq 1+e^{\beta z}$ that holds for all $z \in \mathbb{R}_+$. □

Proof. (Proposition 5.3)

Note that, if $z \geq 0$, $\tanh(z) > 0$, then $\mathbb{R}_+ \subseteq \text{dom}_+(\tanh)$.

$$\tanh'(z) = \frac{4}{(e^z + e^{-z})^2}. \tag{12}$$

Since, if $z \geq 0$ $\tanh'(z) > 0$, what we want to prove is equivalent to $\tanh'(z)z \leq \tanh(z)$. If we plug in the last equation the exponential formulation of the hyperbolic tangent and (12) we get

$$\frac{4z}{e^z + e^{-z}} \leq e^z - e^{-z}.$$

Using the exponential formulation of the hyperbolic sine we obtain

$$2z \leq \sinh(2z).$$

The Taylor expansion of the sinh is

$$\sinh(2z) = 2z + \frac{(2z)^3}{3!} + \frac{(2z)^5}{5!} + \frac{(2z)^7}{7!} + \dots = \sum_{k=0}^{\infty} \frac{(2z)^{2k+1}}{(2k+1)!}.$$

Since the first term of the series is $2z$ and $z \in \mathbb{R}_+$, the inequality is verified. Thus $\tanh \in \text{subhom}_1(\mathbb{R}_+)$. □

Proof. (Proposition 5.5)

First, note that, for each $z \in \mathbb{R}$, $H(z) > 0$, thus $\text{dom}_+(H) = \mathbb{R}$. The Clarke's generalized Jacobian of H respect to x is:

$$\partial H(z) = \begin{cases} 0 & \text{if } z < \alpha_1 \text{ or } z > \alpha_2, \\ [0, 1] & \text{if } z = \alpha_1 \text{ or } z = \alpha_2 \\ 1 & \text{otherwise} \end{cases}$$

Then we get

$$\partial H(z)z = \begin{cases} 0 & \text{if } z < \alpha_1 \text{ or } z > \alpha_2, \\ [0, \alpha_1] & \text{if } z = \alpha_1 \\ [0, \alpha_2] & \text{if } z = \alpha_2 \\ z & \text{otherwise} \end{cases}$$

Thus by the definition of H we obtain the inequality $|Mz| \leq H(z)$ for each $z \in \mathbb{R}$ and for each $M \in \partial H(z)$. □

Subhomogeneous Deep Equilibrium Models

Dataset	Train set size	Validation set size	Test set size
MNIST	71 %	14.5 %	14.5 %
CIFAR-10	70 %	15 %	15 %
SVHN	50.358 %	23.4235 %	26.2184 %

Table 4. Hold out split proportion

	Models Hyperparameter			
	MNIST (Dense)	MNIST (Conv)	Cifar-10	SVHN
Number of input channels (x)	-	1	3	3
Number of hidden channels (z)	-	16	48	48
Size of hidden channels (z)	-	28×28	32×32	32×32
Hidden kernel size hidden (z)	-	3×3	3×3	3×3
Input kernel size (x)	-	3×3	3×3	3×3
Dimension of input weight matrix (x)	784×87	-	-	-
Dimension of hidden weight matrix (z)	87×87	-	-	-
Average pooling	-	4×4	8×8	8×8
Epochs	30	40	40	40
Initial learning rate	10^{-3}	10^{-3}	10^{-3}	10^{-3}
Learning rate schedule	Cosine Annealing	Cosine Annealing	Cosine Annealing	Cosine Annealing
minimum learning rate	10^{-6}	10^{-5}	10^{-3}	10^{-3}
Weight decay	10^{-5}	10^{-5}	10^{-5}	10^{-5}
Batch size	256	256	128	128

Table 5. Models Hyperparameter

Proof. (Proposition 5.6)

We compute the gradient of σ and we get

$$\nabla \sigma(z) = \frac{1}{\sum_i e^{z_i}} [e^{z_1}, \dots, e^{z_n}]^\top = \frac{e^z}{\sum_i e^{z_i}}.$$

Thanks to the convexity of the exponential function we obtain

$$\max_i z_i = \log(e^{\max_i z_i}) \leq \log(e^{\sum_i z_i}) \leq \log\left(\sum_i e^{z_i}\right) = \sigma(z)$$

from the previous inequality we obtain

$$|\nabla \sigma(z)^\top z| = \nabla \sigma(z)^\top z = \frac{\sum_i z_i e^{z_i}}{\sum_i e^{z_i}} \leq \max_i z_i \leq \sigma(z).$$

This shows that $\sigma \in \text{subhom}_1(\mathbb{R}_+^n)$. Thanks to the fact that $\nabla \sigma(z)$ is entrywise positive for each $z \in \mathbb{R}_+^n$, for Remark 3.3, $\sigma \in \text{s-subhom}_1(\mathbb{R}_+^n)$. \square

B. Additional tables

Additional information about training data and training parameters are listed in Table 4 and Table 5.

C. Additional Experiments

We initiate by considering the general equation for a SubDEQ

$$z = \text{norm}_\varphi(\sigma_1(\sigma_2(Wz) + f_\theta(x))).$$

As we illustrate in Section 4, we can build several categories of SubDEQ layer by choosing either σ_1 or σ_2 as the nonlinear activation function. The two SubDEQs proposed in Section 6 have $\sigma_1 = \text{Id}$ and $\sigma_2(z)$ as the activation functions, if we

want to swap σ_1 and σ_2 , so σ_1 be the nonlinear function and σ_2 the identity, we must restrict the hidden weights of our DEQ layers to be positive, since in order to apply Lemma 4.1 $\sigma_2(Wz)$ must be positive in the positive orthant. Two examples of this kind are:

$$\text{norm}_{\|\cdot\|_\infty}(\tanh(|W|z + \text{ReLU}(Ux + b)) + 1.2),$$

and exploiting the power scaling trick

$$\text{norm}_{\|\cdot\|_\infty}(\tanh(|W|z + \text{ReLU}(Ux + b))^{0.99}),$$

where $|W|$ is meant as the absolute value applied entrywise to the weight matrix W . Both layers are well-posed, as their unnormalized versions is subhomogeneous with a degree of 0.99 and differentiable with an entrywise positive Jacobian. We test them on the same dataset used in Section 6.2 using the same training, validation, and test splitting with the same hyperparameter of the SubDEQ models in Section 6.2, in Table 6 we report the misclassification error on the test set.

Model	Error %
MNIST (Dense)	
SubDEQ (ShiftedTanh (1.603))	2.088 ± 0.1405 %
SubDEQ (Tanh)	2.174 ± 0.0595 %
SubDEQ (ShiftedTanh (1.2))	2.437 ± 0.0788 %
SubDEQ (PowerscaledTanh)	2.568 ± 0.0495 %
MNIST (Convolutional)	
SubDEQ (ShiftedTanh (1.603))	1.354 ± 0.98 %
SubDEQ (Tanh)	1.02 ± 0.0642 %
SubDEQ (ShiftedTanh (1.2))	1.829 ± 0.0888 %
SubDEQ (PowerscaledTanh)	1.773 ± 0.1948 %
CIFAR-10	
SubDEQ (ShiftedTanh (1.603))	28.364 ± 0.377 %
SubDEQ (Tanh)	28.166 ± 0.6568 %
SubDEQ (ShiftedTanh (1.2))	35.809 ± 0.5953 %
SubDEQ (PowerscaledTanh)	33.864 ± 0.7469 %
SVHN	
SubDEQ (ShiftedTanh (1.603))	9.3562 ± 0.2122 %
SubDEQ (Tanh)	9.9539 ± 0.5556 %
SubDEQ (ShiftedTanh (1.2))	25.3903 ± 3.7394 %
SubDEQ (PowerscaledTanh)	23.4688 ± 4.7033 %

Table 6. Mean ± standard deviation of the misclassification error on test set

We also conduct other experiments with the graph neural network architecture. In section Section 6.3 we considered the following architecture

$$\begin{cases} \tilde{Z} = \text{norm}_{\|\cdot\|_\infty} \left(\tanh \left((1 - \alpha)\tilde{A}\tilde{Z} \right) + \alpha f_\theta(X) + 1.2 \right) \\ Z = \text{softmax}(\tilde{Z}) \end{cases} \quad (13)$$

Notice that, the map

$$\tilde{Z} \mapsto (1 - \alpha)\tilde{A}\tilde{Z}$$

is 1-subhomogeneous, $\alpha f_\theta(X)$ is a positive translation vector, and $\tanh(\cdot) + 1.2$ is 0.99-storngly subhomogeneous. Thus, $\tanh \left((1 - \alpha)\tilde{A}\tilde{Z} + \alpha f_\theta(X) \right) + 1.2$, due to Lemma 4.1, has a subhomogeneity degree of 0.99, since is differentiable with an entrywise positive Jacobian, the following iteration converge

$$\begin{cases} \tilde{Z} = \text{norm}_{\|\cdot\|_\infty} \left(\tanh \left((1 - \alpha)\tilde{A}\tilde{Z} + \alpha f_\theta(X) \right) + 1.2 \right) \\ Z = \text{softmax}(\tilde{Z}) \end{cases} \quad (14)$$

We test also this architecture on the same dataset used in Section 6.3 comparing it with APPNP and APPNP ShiftedTanh. Moreover, we tune the α parameter making a grid search on the value $[0.05, 0.1, 0.3, 0.5, 0.7, 0.9]$. To tune α we fixed the test set as half of the unknown labels, and we trained the models by varying α . For each model, we select the optimal α by

choosing the one that achieved the highest accuracy on the validation set, the validation set is the half remaining part of the unknown labels. Subsequently, We trained the model five times using the optimal α , altering the training set by sampling from all observations in the dataset that were not part of the initially fixed test set. After each training session, We measured the accuracy of the test set and reported the mean and standard deviation. The results are reported in the table 7, where (14) is APPNP (ShiftedTanh) 2 and (13) is APPNP (ShiftedTanh).

Dataset (% labeled)	Accuracy
Cora citation (7.8 %)	
APPNP	76.3835 ± 0.7716%
APPNP (ShiftedTanh)	73.4996 ± 0.952 %
APPNP (ShiftedTanh) 2	68.978 ± 0.6919 %
Cora author (7.8%)	
APPNP	67.5136 ± 2.8851 %
APPNP (ShiftedTanh)	69.5713 ± 1.3922 %
APPNP (ShiftedTanh) 2	68.1995 ± 2.2836 %
CiteSeer (7.8 %)	
APPNP	61.5763 ± 1.1541 %
APPNP (ShiftedTanh)	59.5334 ± 1.1373 %
APPNP (ShiftedTanh) 2	59.8739 ± 1.6284 %
DBLP (6.0 %)	
APPNP	89.2161 ± 0.216 %
APPNP (ShiftedTanh)	89.545 ± 0.0526 %
APPNP (ShiftedTanh) 2	86.9683 ± 0.1177 %
PubMed (1.2%)	
APPNP	75.9526 ± 0.76875 %
APPNP (ShiftedTanh)	76.9303 ± 0.777 %
APPNP (ShiftedTanh) 2	75.0607 ± 0.70495 %

Table 7. Mean ± standard deviation accuracy on test set